

A Quad-Band Dipole Antenna with Dual I-Shaped Stubs and V-Shaped Etching for Surveying Drone Applications

Suwat Sakulchat¹, Sommart Promput^{2,*}, Watcharaphon Naktong³, and Panuwit Thongbor⁴

¹Department of Electrical Engineering, Faculty of Engineering and Architecture
Rajamangala University of Technology, Suvarnabhumi, Phranakhon Si Ayutthaya 13000, Thailand

²Department of Mechatronics and Robotics Engineering, School of Engineering and Innovation
Rajamangala University of Technology Tawan-ok, Chonburi 20110, Thailand

³Department of Telecommunication Engineering and Digital Innovation, Faculty of Engineering and Technology
Rajamangala University of Technology Isan, Nakhon Ratchasima 30000, Thailand

⁴Department of Electronics and Telecommunication Engineering, Faculty of Engineering
Rajamangala University of Technology Thanyaburi, Pathum Thani 12120, Thailand

ABSTRACT: This research presents a quad-band dipole antenna for use with a surveying drone. The dipole antenna structure design employs the technique of adding I-shaped stubs and V-shaped etching, using aluminum plates with a strong and lightweight structure, with a thickness of 2 mm, a width of 1,325 mm, and a length of 190 mm. The antenna is designed to support frequency bands according to standards (VOR: Very High Frequency Omnidirectional Range) at 118 MHz, (GS: Glide Slope) at 336 MHz, (DME: Distance Measuring Equipment) at 1231 MHz, and WiFi at 2.45 GHz. From the calculations and simulations using the CST program, optimal parameter values were obtained, leading to the fabrication of a prototype antenna and the testing of its antenna properties. The results showed reflection coefficient values of -21.87 dB (108–118 MHz), -12.76 dB (328–336 MHz), -11.99 dB (962–1231 MHz), and -21.79 dB (2400–2480 MHz), which covers the VOR/GS/DME/IEEE 802.11b/g/n standards. The antenna gain values are 1.12, 2.38, 3.76, and 4.00 dBi respectively, with an omnidirectional radiation pattern, and the prototype dipole antenna tested with a drone was found to operate normally in the low frequency range of 108–118 MHz, the first mid frequency range of 328–336 MHz, the second mid frequency range of 962–1231 MHz, and the high frequency range of 2400–2480 MHz.

1. INTRODUCTION

Currently, drones have taken on a role in replacing human labor in terms of safety for surveying high-altitude areas or regions with toxic pollution, as well as for surveying polluted water sources or fire-affected areas. Additionally, there are advantages in terms of reducing survey time, as well as lowering the expensive costs associated with each survey. It can be seen that drones can effectively replace human labor in many areas [1–4]. Currently and in the future, drones are extremely important and indispensable in every country, including Thailand. They are used in tasks such as surveying water sources [5–7], construction sites, traffic, transportation, military operations, police work, filmmaking, agricultural research [8–10], and wildlife surveys [11–13], among others.

In terms of bandwidth used according to standards, the VOR (Very High Frequency Omnidirectional Range) standard frequency is 108–118 MHz [14], the GS (Glide Slope) standard frequency is 328.6–335.4 MHz [15], the DME (Distance Measuring Equipment) standard frequency is 962–1231 MHz, 802.11b/g/n 2.45 GHz (2400–2480 MHz), and for cameras, IEEE 802.11a 5.80 GHz (5150–5750 MHz) is used.

The mentioned frequency band was developed to use only one antenna to help reduce the weight of the drone and can re-

ceive signals from more than one bandwidth. Currently, most antennas available for sale use a single frequency for a single antenna. Since one antenna can have multiple frequencies that do not cover the working frequency, it is also expensive. If a different frequency needs to be used, the antenna must be replaced with a new one that matches the required frequency. From the aforementioned problem, researchers have studied and designed a dipole antenna structure for use with drones, specifically a dipole antenna that meets the VOR/GS [16, 17], VOR/GS/DME [18, 19] standards. But it still cannot support frequencies up to the 802.11b/g/n and 802.11a bands, which can utilize various techniques in antenna design to accommodate higher frequency ranges. Starting with a dipole antenna used in the low-frequency range of 15–45 MHz for ground-penetrating radar (GPR) systems [20], including the design of a microstrip antenna structure used in the 2.45 GHz range [21] and in the wideband of Millimeter wave 26.95 to 29.64 GHz [22]. In the Millimeter wave range of 5.8 GHz and 28 GHz used for the 5G wireless network system [23], in the wideband of 2–4 GHz used for Satellite Communication systems [24], and in the frequency ranges of 2.4 GHz and 5.5 GHz used for 2.4G/5G wireless network systems [25]. A frequency range of 1.090 GHz and 3.5 GHz is used for the 5G wireless network system [26]. Frequency ranges 2.4 GHz and 5.5 GHz are used for drones in the 2.4G/5G system [27]. Millimeter-wave in the frequency range

* Corresponding author: Sommart Promput (sommart_pr@rmutto.ac.th).

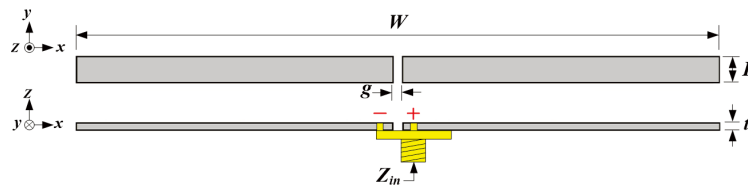


FIGURE 1. The basic dipole antenna.

of 26.63–29.91 GHz is used [28]. Additionally, the antenna structure is designed as a monopole antenna, used in the 5G mobile communication system within the frequency range of 3.4–3.8 GHz. It is utilized for advanced biomedical applications such as unmanned aerial vehicles (UAVs), autonomous vehicles (AVs), and swarm drones (SDA) [29]. Used in the 5G mobile communication system, operating on dual-band: 5.2 GHz and 5.8 GHz. Used for drones in the 5G WLAN system, it can be utilized for search and rescue, tracking, surveillance, emergency assistance, delivery, and aerial photography and videography [30]. An ellipse-shaped monopole antenna for installation at the front of the drone is used in 5G communication systems with an operating frequency range of 3.5 GHz [31]. A horn antenna is installed at the back of the drone and used in communication systems surrounded by environmental conditions (radomes, ground obstacles, metal supports, rain, temperature gradients, rain, snow, ice, dirt, etc.) with an operating frequency range of 3–32 GHz and a gain value ranging from 2.2–15.5 dB [32]. The horn antenna is installed at the back of the drone. It is used in interferometric synthetic aperture radar (InSAR), an active remote sensing technique that generally uses satellite data to measure the deformation of the Earth's surface. It operates in the frequency range of 5.4 GHz with a gain of 19 dBi [33].

Based on the aforementioned, the researcher is interested in developing a single dipole antenna to support the navigation system of aircraft, capable of operating in three main frequency bands: VOR, GS, DME, and WiFi 2.45 GHz, which are standard frequencies used for monitoring aircraft takeoff and landing. The choice to design a dipole antenna is due to its omnidirectional radiation pattern, making it suitable for installation on drones and easy to tune to different frequencies [16–20]. In comparison to other types of antennas, such as arrays and waveguides [29–33], which have specific radiation patterns and are more difficult to tune the antenna structure. Additionally, the prototype dipole antenna will be developed to be lightweight and resistant to flight conditions. The process of tuning the antenna structure to operate at the desired frequency will be covered in Section 2. Section 3 will present the fabrication and measurement of the antenna. Section 4 will compare the performance of the developed antenna with other types of antennas. Finally, the last section will summarize the overall research findings.

2. ANTENNA DESIGN AND SIMULATION

The design of the planar dipole antenna will be based on an aluminum structure because it is lightweight, inexpensive, and rust-resistant. Aluminum sheets with a thickness (t) of 2 mm

will be used, with an aluminum conductivity of (σ) = 3.56×10^7 S/m, which has low loss. This antenna is designed to operate by tuning to the resonance frequency in the initial frequency range of 113 MHz, which is used in the navigation system within the frequency range of 108–118 MHz (Very High Frequency Omnidirectional Range: VHF-OR). According to this standard, it is suitable for use in drones. In the design calculation of the antenna structure, the width is derived from Equation (1), the length from Equation (2), and the distance between the positive and negative terminals from Equation (3), which are based on the resonance frequency and the material constants. The calculated width (W) is 1,325 mm. The length (L) is equal to 40 mm. And the distance (g) is equal to 2 mm, as shown in Figure 1. The dipole antenna structure is designed for a low frequency of 113 MHz within the low frequency range of 108–118 MHz, which has an impedance bandwidth of 50 ohms. The properties of aluminum are as follows:

$$W = 0.5\lambda \quad (1)$$

$$L = 0.015\lambda \quad (2)$$

$$g = 0.00075\lambda \quad (3)$$

After obtaining the values from the calculations, the dipole antenna structure was simulated using the CST program. It was found that the reflection coefficients $|S_{11}|$ responded at the frequency range of 113 MHz at point A1, but there was no response in the frequency range of 332 MHz at point A2, 1096.5 MHz and 2450 MHz, as shown in Figure 2(a). Therefore, the antenna structure was tuned to respond to additional frequencies, starting with 332 MHz. By analyzing the current density at the 332 MHz frequency range, it was found that the current density was consistent throughout the middle section at the feed point, as shown in Figure 2(b). The researchers then employed adding stub and etching techniques to help tune the antenna structure, which will be discussed in the next section.

The steps for simulating the tuning of a dipole antenna structure to respond to the desired frequency range will involve six steps. This is to ensure that the characteristic impedance obtained from the experimental method, combined with the electrical simulation program, yields an appropriate reflection coefficient (dB). This will explain the tuning of the dipole antenna structure in the next steps. In the first step, tuning will be done using the adding stub technique [18, 19] to achieve the desired frequency range of 332 MHz, as shown in Figure 3.

The parameter values used the optimal width (W_1) of 40 mm and the tuning length (L_1) adjusted from 170, 180, 190, 200, and 210 mm. The tuning found that the optimal value was a length (L_1) of 190 mm, which had a tuning wavelength of $0.0442\lambda < L_1 < 0.2324\lambda$. The width (W_1) can be calculated

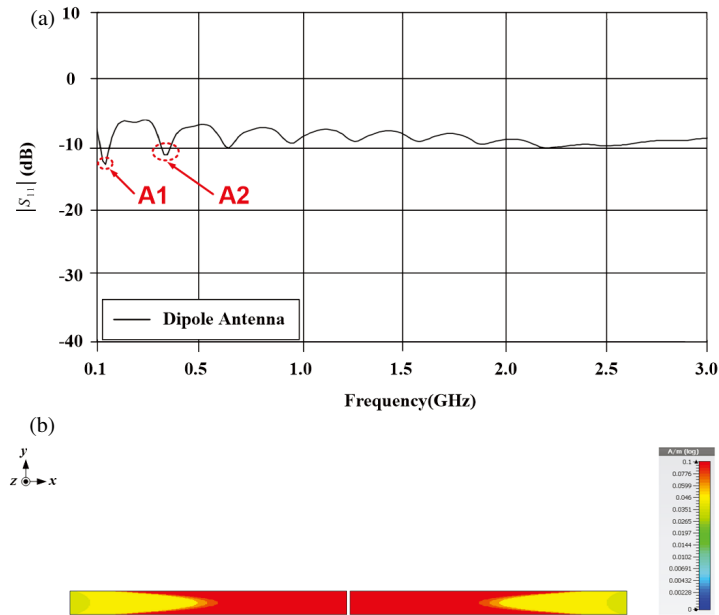


FIGURE 2. The simulation result of basic dipole antenna, (a) reflection coefficient $|S_{11}|$ (dB) and (b) current density.

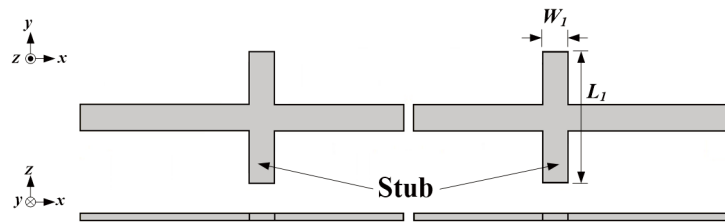


FIGURE 3. The dipole antenna in the first step.

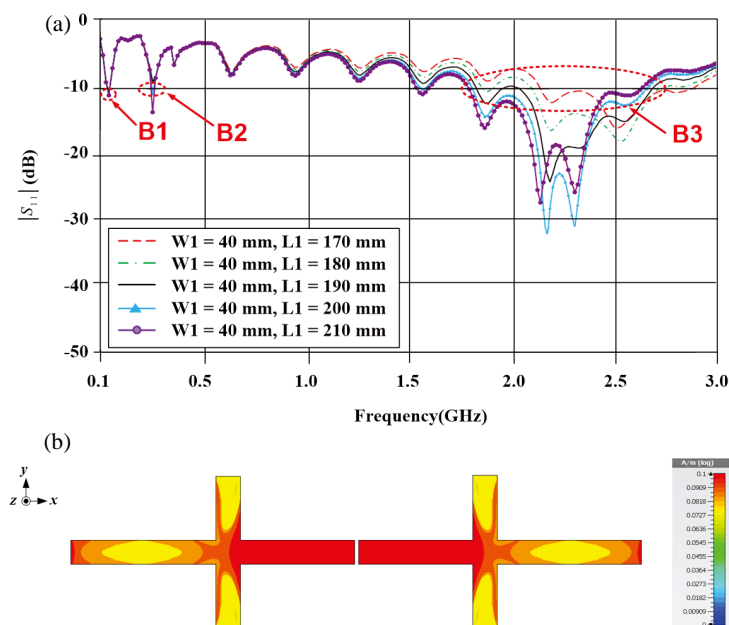


FIGURE 4. The simulation result of the dipole antenna in the first step, (a) reflection coefficient $|S_{11}|$ (dB) and (b) current density.

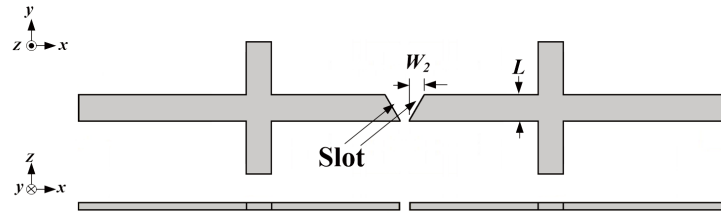
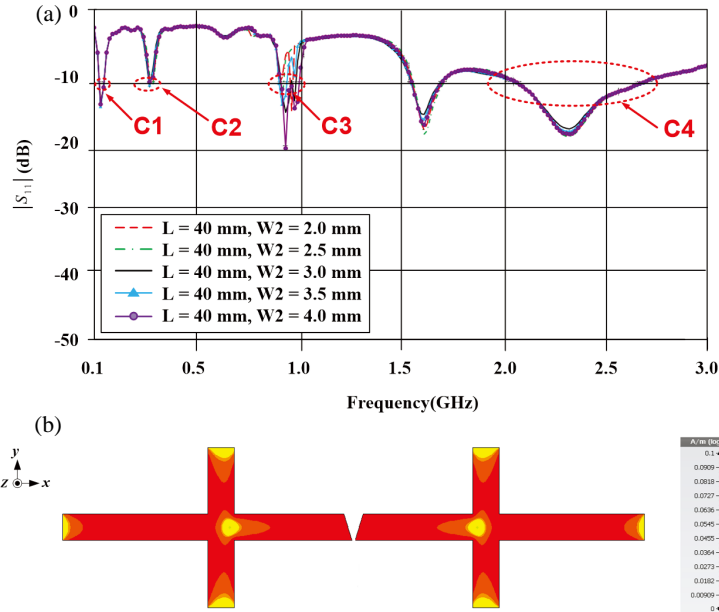


FIGURE 5. The dipole antenna in the second step.

FIGURE 6. The simulation result of the dipole antenna in the second step, (a) reflection coefficient $|S_{11}|$ (dB) and (b) current density.

as per Equation (4) and the length (L_1) as per Equation (5), with the frequency range of 113 MHz at point B1 and 332 MHz at point B2, and the frequency range of 2450 MHz at point B3 responding with a reflection coefficient of $|S_{11}| \leq -10$ (dB). However, it does not respond at the desired frequency range of 1096.5 MHz, as shown in Figure 4(a). Therefore, the current density was simulated at a frequency of 1096.5 MHz, and it was found that the signal feed point had the highest current density, as shown in Figure 4(b). The researchers then used the etching technique to assist in tuning in the next step.

$$W_1 = 0.442\lambda \quad (4)$$

$$L_1 = 0.2102\lambda \quad (5)$$

The second step is to tune using the scalene triangle etching technique [18] at the antenna feed point to make the antenna respond to the frequency range of 1096.5 MHz. This was considered in conjunction with the direction of the current at the antenna feed point, which had the most significant effect as desired, resulting in a shape resembling the letter V, as shown in Figure 5.

From the tuning, it was found that the optimal parameter value for length (L) is 40 mm, and for width (W_2), the tuning selected values of 2, 2.5, 3, 3.5, and 4 mm. By tuning, it was found that the optimal value is a width (W_2) of 3 mm, which has a tuning wavelength of $0.0073\lambda < W_1 < 0.0146\lambda$. The width

can be calculated using Equation (6). The frequency range of 113 MHz at point C1, the frequency range of 1096.5 MHz at point C3, and the frequency range of 2450 MHz at point C4 respond with a reflection coefficient of $|S_{11}| \leq -10$ (dB) and have a negative effect at the frequency range of 332 MHz at point C2, as shown in Figure 6(a). Therefore, an analysis of the current density at the frequency range of 332 MHz was conducted, revealing that the signal feed point had the highest current density throughout the end section, as shown in Figure 6(b). The researchers then applied the stub tuning technique to assist in the next adjustment step.

$$W_2 = 0.011\lambda \quad (6)$$

In the third step, tune using the technique of adding I-shaped stubs on both sides [18, 19], considering in conjunction with the direction of the current at the tip of the antenna, which has the most significant impact, to achieve the desired response at the frequency range of 332 MHz, as shown in Figure 7.

From the tuning, it was found that the optimal parameter value for width (W_3) is 40 mm, and for length (L_2), the tuning options were 150, 160, 170, 180, and 190 mm. The tuning revealed that the optimal value is a length (L_2) of 170 mm, which corresponds to a tuning wavelength of $0.166\lambda < W_1 < 0.2102\lambda$. By showing the frequency range of 113 MHz at point

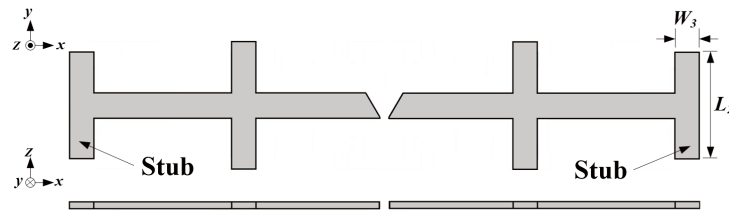


FIGURE 7. The dipole antenna in the third step.

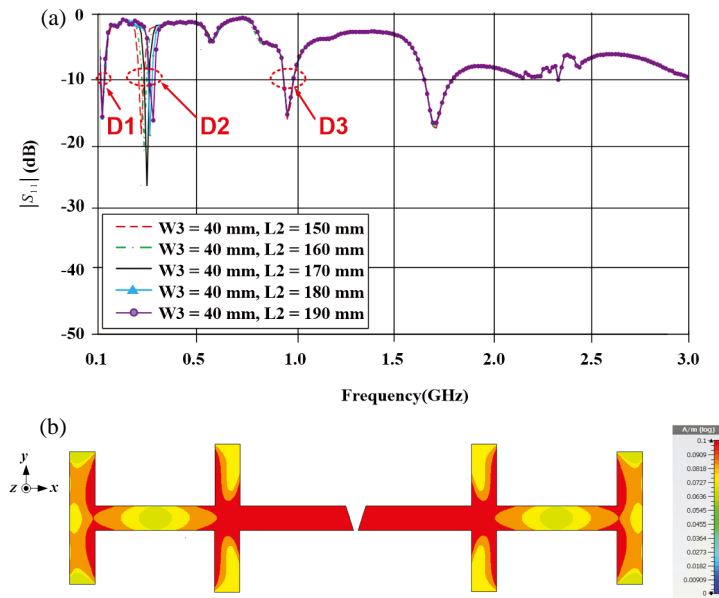


FIGURE 8. The simulation result of the dipole antenna in the third step, (a) reflection coefficient $|S_{11}|$ (dB) and (b) current density.

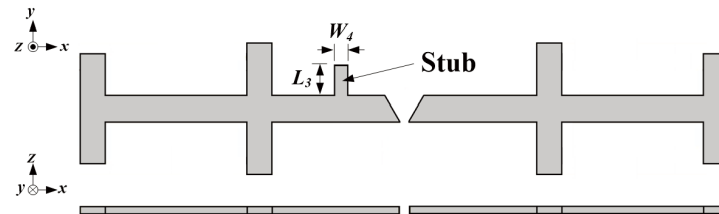


FIGURE 9. The dipole antenna in the fourth step.

D1, 332 MHz at point D2, and 1096.5 MHz at point D3, they respond with a reflection coefficient of $|S_{11}| \leq -10$ (dB).

The width of W_3 can be calculated using Equation (7), and the length of L_2 can be calculated using Equation (8). However, there is a negative effect on the frequency range of 2450 MHz as desired, as shown in Figure 8(a). Therefore, the analysis of current density at the frequency range of 2450 MHz was conducted, which revealed that the area directly above the negative terminal of the antenna had the most significant impact, as shown in Figure 8(b). The researchers then applied the stub tuning technique to assist in the next adjustment step.

$$W_3 = 0.0442\lambda \quad (7)$$

$$L_2 = 0.1881\lambda \quad (8)$$

In the fourth step, tune using the I-shaped stub adding technique [16] by considering the direction of the current in the area directly above the negative terminal of the antenna, which has the most significant impact, to achieve the desired response at the frequency range of 2450 MHz, as shown in Figure 9.

From the tuning, it was found that the optimal parameter value for width (W_4) is 25 mm, and for length (L_3), the tuning options were 35, 40, 45, 50, and 55 mm. The tuning revealed that the optimal length (L_3) value is 45 mm, which corresponds to a tuning wavelength of $0.2858\lambda < L_3 < 0.4491\lambda$. The frequency range of 113 MHz at point E1, 332 MHz at point E2, and 2450 MHz at point E3 respond with a reflection coefficient of $|S_{11}| \leq -10$ (dB), as shown in Figure 10(a). The width can be calculated using Equation (9), and the length can be calculated using Equation (10). However, it hurt the desired

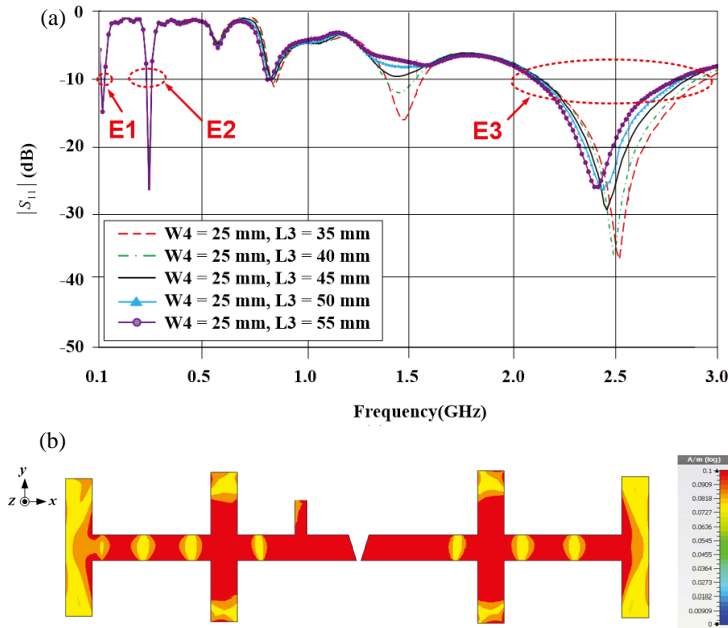


FIGURE 10. The simulation result of the dipole antenna in the fourth step, (a) reflection coefficient $|S_{11}|$ (dB) and (b) current density.

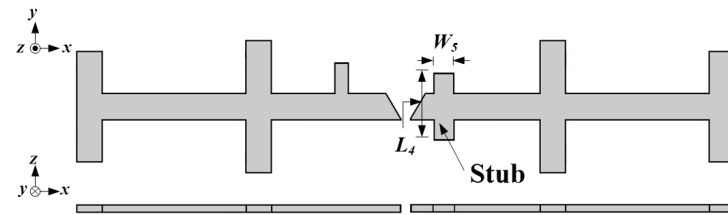


FIGURE 11. The dipole antenna in the fifth step.

frequency band of 1,096.5 MHz. Therefore, the current density at the 1,096.5 MHz frequency band was analyzed, and it was found that the area directly above, near the positive terminal of the antenna, had the most significant impact, as shown in Figure 10(b).

$$W_4 = 0.2041\lambda \quad (9)$$

$$L_3 = 0.3675\lambda \quad (10)$$

In the fifth step, tune using the I-shaped stub adding technique by considering in conjunction with the direction of the current near the positive terminal of the antenna [16], which has the most significant impact, to achieve the desired response at the frequency range of 1096.5 MHz, as shown in Figure 11.

From the tuning, it was found that the optimal parameter value for width (W_5) is 25 mm, and for length (L_4), the tuning options were 90, 100, 110, 120, and 130 mm. The tuning revealed that the optimal value for length (L_4) is 110 mm, which corresponds to a tuning wavelength of $0.3289\lambda < L_4 < 0.4751\lambda$. The width of W_5 can be calculated as per Equation (11) and the length of L_4 as per Equation (12), with the frequency range of 113 MHz at point F1, the frequency range of 332 MHz at point F2, and the frequency range of 1096.5 MHz at point F3 responding with a reflection coefficient of $|S_{11}| \leq -10$ (dB). However, it has a negative effect on the frequency range of 2450 MHz at point F4 again, as shown in Figure 12(a).

Therefore, the analysis of the current density at the frequency range of 2450 MHz was conducted, which revealed that the area directly above the negative terminal of the antenna, had the most significant impact, as shown in Figure 12(b). The researcher then used stub adding techniques to assist in tuning for the next step.

$$W_5 = 0.0913\lambda \quad (11)$$

$$L_4 = 0.4020\lambda \quad (12)$$

In the sixth step, tune using the I-shaped stub adding technique, considering the direction of the current in the area directly above the antenna's negative terminal [16], which has the most significant impact. This is done to achieve the desired response in the 2450 MHz frequency range, as shown in Figure 13.

From the tuning, it was found that the optimal parameter value for width (W_6) is 6 mm, and for length (L_5), the tuning was adjusted to 10, 12.5, 15, 17.5, and 20 mm. The tuning revealed that the optimal value for length (L_5) is 15 mm, which corresponds to a tuning wavelength of $0.0816\lambda < L_5 < 0.1633\lambda$. The width (W_6) can be calculated as per Equation (13) and the length (L_5) as per Equation (14), with the frequency range of 113 MHz at point G1, 332 MHz at point G2, 1096.5 MHz at point G3, and 2450 MHz at point G4, achieving a reflection coefficient of $|S_{11}| \leq -10$ (dB) as desired, as

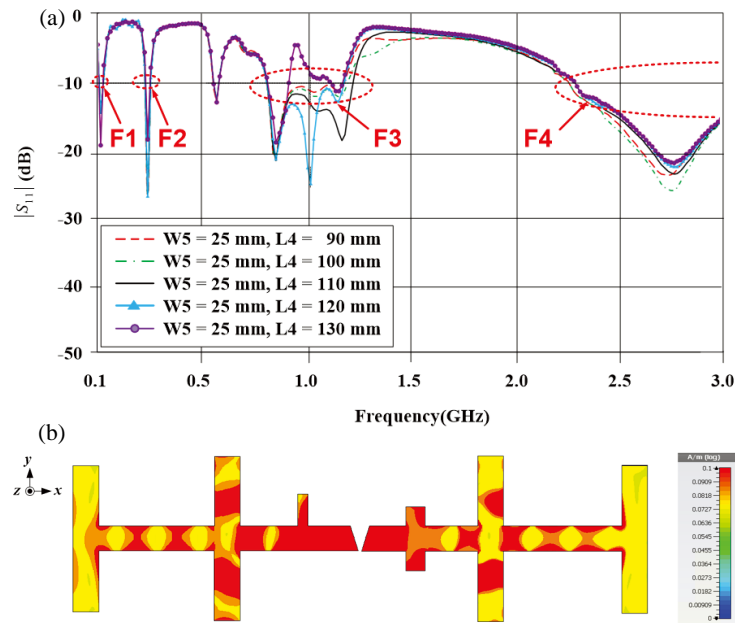


FIGURE 12. The simulation result of the dipole antenna in the fifth step, (a) reflection coefficient $|S_{11}|$ (dB) and (b) current density.

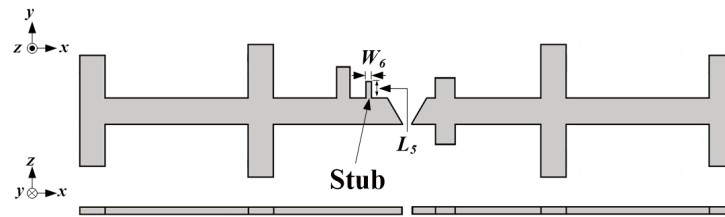


FIGURE 13. The dipole antenna in the sixth step.

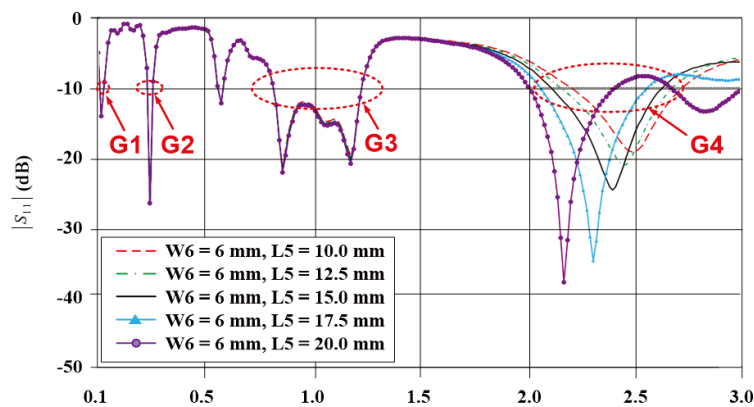


FIGURE 14. The simulation result of reflection coefficient $|S_{11}|$ (dB) in the sixth step.

shown in Figure 14.

$$W_6 = 0.049\lambda \quad (13)$$

$$L_5 = 0.1225\lambda \quad (14)$$

The structure of the dipole antenna obtained from calculations and simulations using the CST program, which relies on adding stub and etching techniques based on experimental methods to find various parameters until the most suitable parameters for drone applications are achieved, as shown in Fig-

ure 15 and Table 1, results in an impedance bandwidth response across four bandwidths as desired, as shown in Table 2.

From the simulation of the dipole antenna structure using aluminum plates, the antenna structure was modified in 6 steps. Adding I-shaped stubs combined with triangular etching resulted in operational frequency ranges of 108–118 MHz, 328–336 MHz, 962–1231 MHz, and 2400–2480 MHz. Each of these four ranges has antenna gain values of 0.69, 2.33, 4.17, and

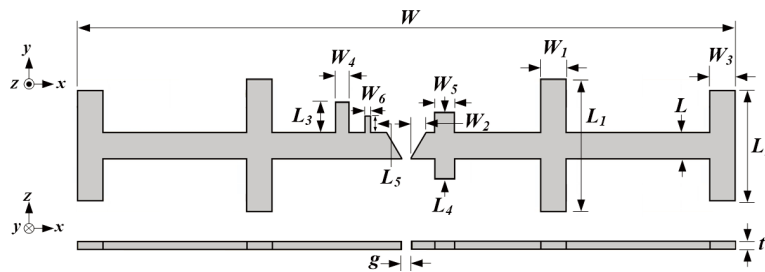


FIGURE 15. The proposed dipole antenna structure.

TABLE 1. The optimal parameters of the dipole antenna for the final tuning step.

Parameter	Description	Size (mm)
W	The width of dipole antenna	1,325
W_1	The width of dual I-shaped stub of the first step	40
W_2	The width of V-shape at feed point of the second step	3
W_3	The width of dual I-shaped stub of the third step	40
W_4	The width of I-shaped stub at negative terminal	25
W_5	The width of I-shaped stub at positive terminal	30
W_6	The width of I-shaped stub at the edge of negative terminal	6
L	The length of dipole antenna	40
L_1	The length of dual I-shaped stub of the first step	190
L_2	The length of dual I-shaped stub of the third step	170
L_3	The length of I-shaped stub at negative terminal	45
L_4	The length of I-shaped stub at positive terminal	60
L_5	The length of I-shaped stub at the edge of negative terminal	50
g	Gap between positive and negative feed point	2
t	The thickness of aluminum sheet	2

TABLE 2. Comparison of properties of all antenna.

Frequency (MHz)	$ S_{11} $ (dB)	VSWR	Impedance (Ω)	Gain (dBi)	f_c (MHz)	Bandwidth (MHz)	BW (%)
113	-13.13	1 : 1.72	$55.74 - j24.14 \Omega$	0.69	117.5	118–127	16.17
332	-25.71	1 : 1.21	$44.22 - j1.95 \Omega$	2.33	333.5	320–347	8.10
1096.5	-14.22	1 : 1.48	$44.82 - j18.07 \Omega$	4.17	1088.85	890–1287.7	36.52
2450	-22.70	1 : 1.16	$57.35 - j2.71 \Omega$	5.11	2387	2141–2633	20.61

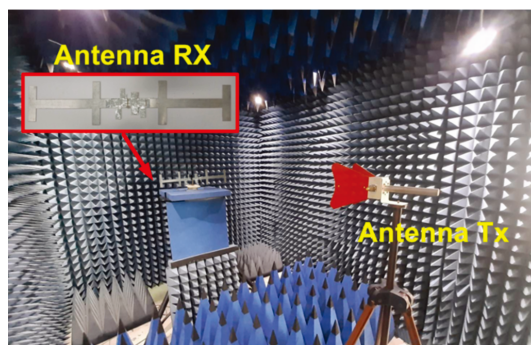


FIGURE 16. Preparing proposed dipole antenna in a chamber room.

5.11 dBi, respectively, and exhibits omnidirectional radiation patterns across all frequency bands.

3. ANTENNA FABRICATION AND MEASUREMENT

After simulating the antenna structure until the parameters were optimized, a dipole antenna was fabricated using aluminum sheets, as shown in Figure 16. The antenna's properties were then measured using a network analyzer. It was found that the dipole antenna performed well across several frequency ranges, particularly in the frequency bands used for drone communication, namely 113 MHz, 332 MHz, 1096.5 MHz, and 2450 MHz, which aligns with the results from the simulation, as illustrated in Figure 17. The antenna has a relatively wide bandwidth in each frequency range, allowing it to support signals across var-

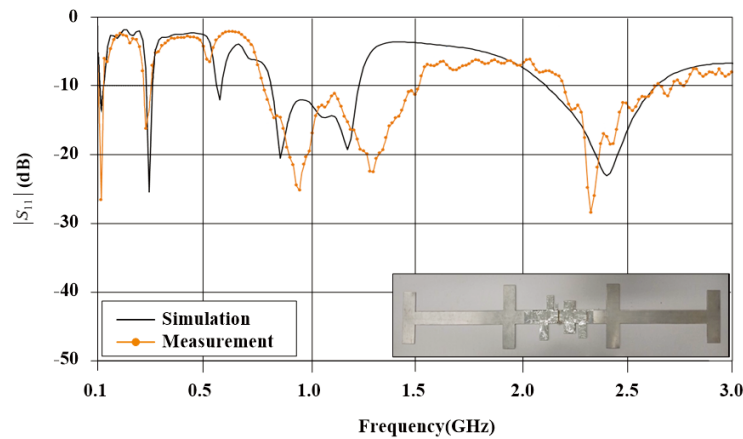


FIGURE 17. Comparison of reflection coefficient $|S_{11}|$ between simulation and measurement results.

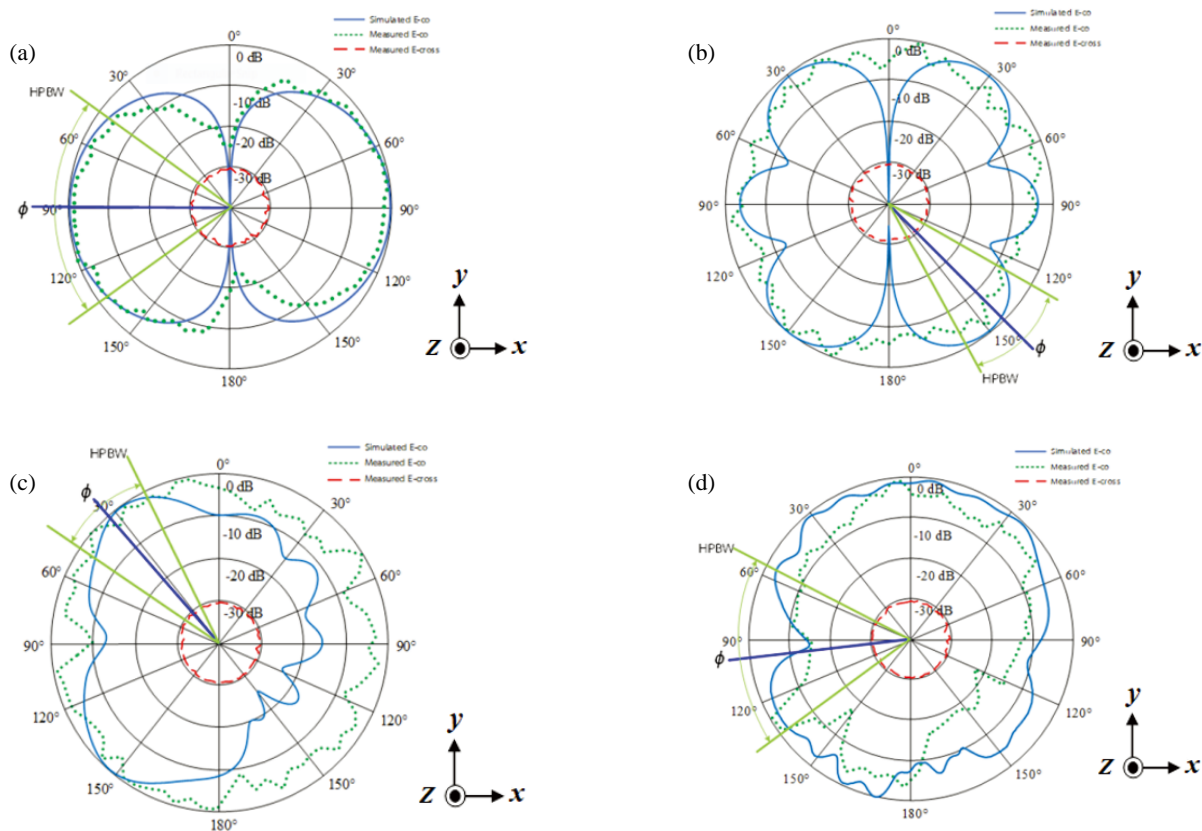


FIGURE 18. Comparison of E -plane between simulation and measurement result at (a) 113 MHz, (b) 332 MHz, (c) 1096.5 MHz, and (d) 2450 MHz.

ious frequencies. The VSWR value is 1.44 : 1, which is within an acceptable range, and the impedance value is close to the standard 50Ω , indicating that the antenna can match well with the system. The antenna has an omnidirectional radiation pattern, making it suitable for various applications. The antenna gain increases with higher frequencies in succession, as shown in Table 3.

The measurement results of the E -plane radiation patterns compared to the simulation results at the frequency range of 113 MHz and 332 MHz show bidirectional radiation patterns. The frequency ranges of 1096.5 MHz and 2450 MHz exhibit omnidirectional radiation patterns, which trend in the same di-

rection as shown in Figure 18. The measurement results of the main lobe direction and the half power beam width (HPBW) are presented in Table 4.

The measurement results of the H -plane radiation pattern compared to the simulation results at frequencies of 113 MHz, 332 MHz, 1096.5 MHz, and 2450 MHz show an omnidirectional radiation pattern, which tends to follow the same direction as shown in Figure 19. The measurement results of the main lobe direction and half power beam width (HPBW) are presented in Table 4.

The prototype antenna made from aluminum sheets weighs 0.68 kg, which is designed to operate in four bandwidths and

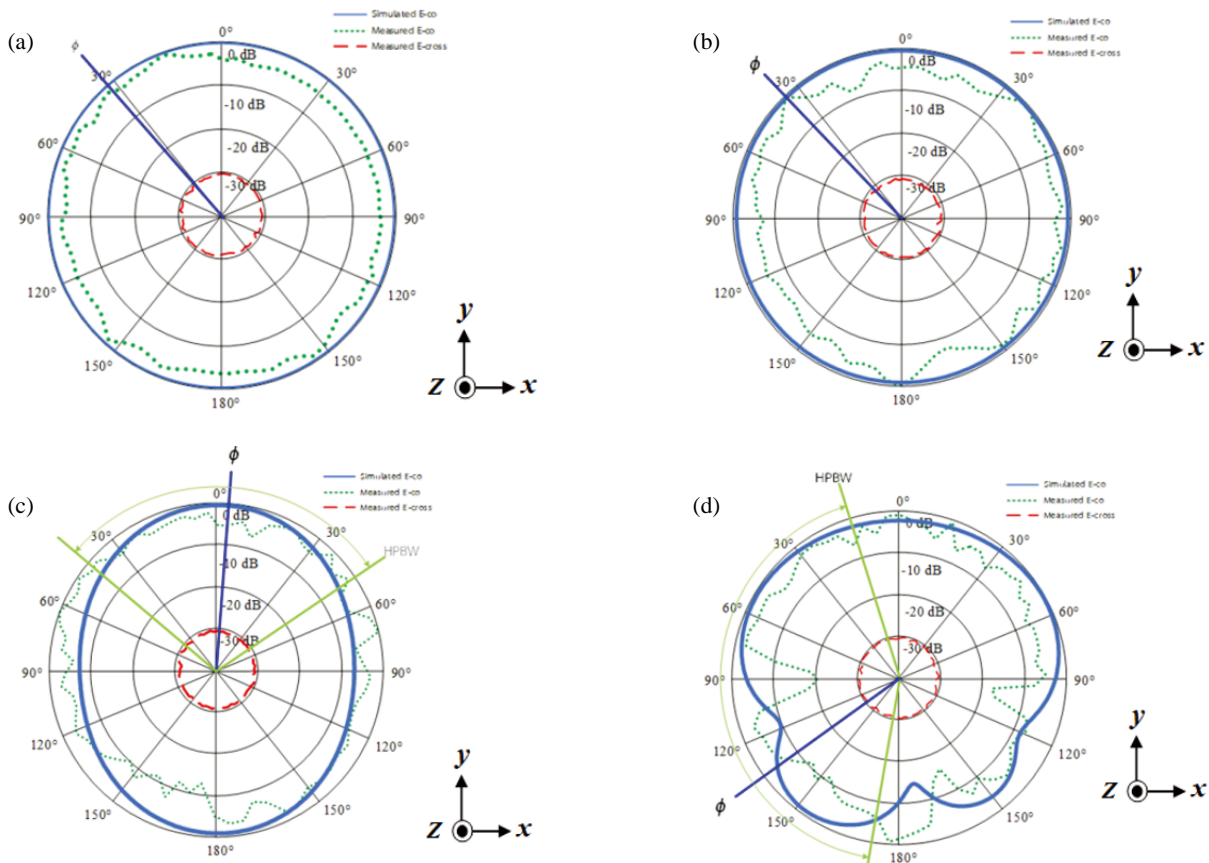


FIGURE 19. Comparison of H -plane between simulation and measurement result at (a) 113 MHz, (b) 332 MHz, (c) 1096.5 MHz and (d) 2450 MHz.

TABLE 3. Comparison of properties of all antenna.

Results	f_r (MHz)	$ S_{11} $ (dB)	f_c (MHz)	BW (MHz)	Bandwidth (%)	VSWR	Z_{in} (Ω)	Gain (dBi)
Measured	113	-21.87	119.50	109–130	17.57	1.20 : 1	$44.76 + j21.56$	1.12
	332	-12.76	330	318–342	7.27	1.55 : 1	$41.14 - j2.32$	2.38
	1096.5	-11.99	1292	883–1701	63.31	1.68 : 1	$62.55 + j10.59$	3.76
	2450	-21.79	2487	2290–2684	15.84	1.16 : 1	$53.95 - j4.38$	4.00



FIGURE 20. Mounting the prototype antenna on drone.



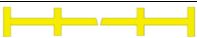
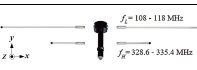


with an omnidirectional radiation pattern. It is used with a drone by positioning the antenna in the H -plane as shown in Figure 20. For preliminary functional testing, the drone operates at a low frequency range of 113 MHz, first mid frequency

TABLE 4. The main lobe direction and half power beam width (HPBW) of E - and H -plane.

Frequency (MHz)	Main lobe		Half power beam width	
	E -p	H -p	E -p	H -p
113	90°	7°	81.30°	—
332	218°	32°	34.30°	—
1096.5	33°	2°	31.00°	93.8°
2450	99°	133°	87.30°	156°

range of 332 MHz, second mid frequency range of 1096.5 MHz, and high frequency range of 2450 MHz. It was found that this prototype antenna can respond in all desired frequency ranges.

TABLE 5. Comparison of proposed antenna with previous antenna in VOR/GS/DME/802.11b/g/n standard.

Reference	Antenna Structure	Standard	Gain(dBi)	Material	Size(mm ³)	Weight(kg)
[16]		VOR/GS	5.98/8.76	Aluminum	300x300x2	0.9
[17]		VOR/GS	2.13/3.21	FR4	40x700x1.7	0.25
[18]		VOR/GS/DME	0.69/2.33/4.17	Aluminum	170x1,325x2	0.52
[19] (Original)		VOR/GS	-	Aluminum	30x1200x10	1.8
[19]		VOR/GS/DME	1.73/3.43/6.31	FR4	144x633x1.7	0.4
Proposed Antenna		VOR/GS/DME/802.11b/g/n	1.12/2.38/3.76/4	Aluminum	190x1,325x2	0.68

4. DISCUSSION

In terms of comparing the performance of the antenna with previous research in VOR/GS/DME/802.11b/g/n standard, it was found that the aluminum dipole antenna structure tuned with dual I-shaped stubs and V-shaped etching has a simpler tuning point than the research in [19]. Additionally, the aluminum structure is lighter than the research in [16, 19] (original) and provides better rust prevention than the research in [17, 19]. Furthermore, it covers four frequency bands for usage, more than the research in [16–19], as shown in Table 5.

5. CONCLUSION

This research presents a dipole antenna designed from light weight aluminum plates, tuned with a dual-I shaped stubs and V-shaped etching, for use with surveying drones. Through calculations and simulations using the CST program, suitable parameters were obtained. When a prototype antenna is fabricated, and the antenna properties were measured, the reflection coefficient values were found to be -21.87 dB (for the low resonance frequency range of 108–118 MHz), -12.76 dB (for the first mid resonance frequency range of 328–336 MHz), -11.99 dB (for the second mid resonance frequency range of 962–1231 MHz), and -21.79 dB (for the high resonance frequency range of 2400–2480 MHz), which cover the VOR/GS/DME/IEEE 802.11b/g/n standards. The antenna gain values of 1.12, 2.38, 3.76, and 4.00 dBi, respectively, and an omnidirectional radiation pattern across all frequency bands, the measurement results are consistent with the simulation. The prototype antenna was tested for preliminary functional experiments with a surveying drone, which can respond in all desired frequency ranges. The structure of this prototype antenna has several significant advantages, including simple design, the use of low-cost materials, and resistance to rust. Additionally, the prototype antenna has a response that covers all frequency ranges more than previous research and has a gain sufficient for use, which can be applied to RF energy harvesting systems at airports using VOR/GS/DME/IEEE 802.11b/g/n standards in the future.

ACKNOWLEDGEMENT

The authors would like to thank the Department of Telecommunication Engineering and Digital Innovation, Faculty of Engineering and Technology, Rajamangala University of Technology Isan, for providing equipment and research funding. Department of Electrical Engineering, Faculty of Engineering and Architecture, Rajamangala University of Technology Suvarnabhumi, to support the sample of raw materials and equipment. Department of Electronics and Telecommunication Engineering, Faculty of Engineering, Rajamangala University of Technology Thanyaburi, for supporting this work with the simulation CST software, and Department of Mechatronics and Robotics Engineering, School of Engineering and Innovation, Rajamangala University of Technology Tawan-ok, for supporting the experimental site.

REFERENCES

- [1] Tariq, R., M. Rahim, N. Aslam, N. Bawany, and U. Faseeha, "DronAID: A smart human detection drone for rescue," in *2018 15th International Conference on Smart Cities: Improving Quality of Life Using ICT & IoT (HONET-ICT)*, 33–37, Islamabad, Pakistan, 2018.
- [2] Herdel, V., L. J. Yamin, and J. R. Cauchard, "Above and beyond: A scoping review of domains and applications for human-drone interaction," in *Proceedings of the 2022 CHI Conference on Human Factors in Computing Systems*, 1–22, New Orleans, United States, 2022.
- [3] Auda, J., M. Weigel, J. R. Cauchard, and S. Schneegass, "Understanding drone landing on the human body," in *Proceedings of the 23rd International Conference on Mobile Human-Computer Interaction*, 1–13, France, 2021.
- [4] Brophy, P., G. Albeaino, M. Gheisari, and I. Jeelani, "New risks for workers at heights: Human-drone collaboration risks in construction," *Computing in Civil Engineering*, 321–328, 2022.
- [5] Rødtang, E., K. Alfreðsen, and A. Juárez, "Drone surveying of volumetric ice growth in a steep river," *Frontiers in Remote Sensing*, Vol. 2, 767073, 2021.
- [6] Sladonja, B., D. Damijanić, M. Krapac, M. Uzelac, I. Linić, and D. Poljuha, "Development of drone-based methodology for inventory and monitoring invasive plants along river banks in croatia," *Management of Biological Invasions*, Vol. 13, No. 4, 679–

- 689, 2022.
- [7] Sanjou, M., K. Kato, W. Aizawa, and T. Okamoto, "Development of drone-type float for surface-velocity measurement in rivers," *Environmental Fluid Mechanics*, Vol. 22, No. 4, 955–969, 2022.
 - [8] Mustamu, N. E., V. Sihombing, *et al.*, "Drone simulation for agriculture and lora based approach," *Internet of Things and Artificial Intelligence Journal*, Vol. 1, No. 4, 221–235, 2021.
 - [9] Ghazali, M. H. M., A. Azmin, and W. Rahiman, "Drone implementation in precision agriculture — A survey," *International Journal of Emerging Technology and Advanced Engineering*, Vol. 12, No. 4, 67–77, 2022.
 - [10] Chin, R., C. Catal, and A. Kassahun, "Plant disease detection using drones in precision agriculture," *Precision Agriculture*, Vol. 24, No. 5, 1663–1682, 2023.
 - [11] Wood, S. A., P. W. Robinson, D. P. Costa, and R. S. Beltran, "Accuracy and precision of citizen scientist animal counts from drone imagery," *PLoS One*, Vol. 16, No. 2, e0244040, 2021.
 - [12] Jintasuttisak, T., A. Leonce, M. S. Shah, T. Khafaga, G. Simkins, and E. Edirisinghe, "Deep learning based animal detection and tracking in drone video footage," in *Proceedings of the 8th International Conference on Computing and Artificial Intelligence*, 425–431, Tianjin, China, 2022.
 - [13] Schad, L. and J. Fischer, "Opportunities and risks in the use of drones for studying animal behaviour," *Methods in Ecology and Evolution*, Vol. 14, No. 8, 1864–1872, 2023.
 - [14] Kawabata, K. and A. Hiroyuki, "Wind influence of air wire antenna suspended from drone," in *2018 International Symposium on Antennas and Propagation (ISAP)*, 1–2, Busan, Korea (South), 2018.
 - [15] Chen, J., D. Raye, W. Khawaja, P. Sinha, and I. Guvenc, "Impact of 3D UWB antenna radiation pattern on air-to-ground drone connectivity," in *2018 IEEE 88th Vehicular Technology Conference (VTC-Fall)*, 1–5, Chicago, IL, USA, 2018.
 - [16] Namsang, A., R. Lerdwanittip, and A. Ruengwaree, "I-shaped antenna with horizontal I-shape tuning for dual-band frequency," in *Proceedings of the 11th Conference of Electrical Engineering Network of Rajamangala University of Technology 2019 (EENET 2019)*, Thailand, 2019.
 - [17] Naktong, W., S. Sakulchat, and L. Ruengyote, "Study of a dipole antenna tuned by triangle-shaped slot for drone," in *The 10th Engineering, Science, Technology and Architecture Conference 2019 (ESTACON 2019)*, 708–713, Thailand, 2019.
 - [18] Naktong, W., M. Kupimai, and S. Wangkuntod, "The studies of a dipole antenna by tuning of I-shape stub for drones application in airport," in *The 12th Engineering, Science, Technology and Architecture Conference 2021 (ESTACON 2021)*, 216–221, Thailand, 2021.
 - [19] Naktong, W., A. Ruengwaree, S. Sakulchat, and S. Prompt, "The design of a triple-band H- and dual C-shaped planar dipole antenna for a drone application," *Progress In Electromagnetics Research C*, Vol. 134, 103–117, 2023.
 - [20] Wu, K. and S. Lambot, "Analysis of low-frequency drone-borne GPR for root-zone soil electrical conductivity characterization," *IEEE Transactions on Geoscience and Remote Sensing*, Vol. 60, 1–13, 2022.
 - [21] Reyna, A., J. C. Garza, O. Elizarraras, M. Panduro, L. I. Balderas, and M. de la Luz Prado, "3D random virtual antenna arrays for FANETs wireless links," *Telecommunication Systems*, Vol. 77, No. 3, 469–477, 2021.
 - [22] Assimonis, S. D., M. A. B. Abbasi, and V. Fusco, "Millimeter-wave multi-mode circular antenna array for uni-cast multi-cast and OAM communication," *Scientific Reports*, Vol. 11, No. 1, 4928, 2021.
 - [23] Imran, A. Z. M., M. L. Hakim, M. R. Ahmed, M. T. Islam, and E. Hossain, "Design of microstrip patch antenna to deploy unmanned aerial vehicle as UE in 5G wireless network," *International Journal of Electrical and Computer Engineering (IJECE)*, Vol. 11, No. 5, 4202–4213, 2021.
 - [24] Zarbakhsh, S. and A. R. Sebak, "Multifunctional drone-based antenna for satellite communication," *IEEE Transactions on Antennas and Propagation*, Vol. 70, No. 8, 7223–7227, 2022.
 - [25] Garza, J. C., A. Reyna, L. I. Balderas, M. A. Panduro, and L. Y. García, "Dual-band virtual antenna array with time modulation in presence of position perturbations," *Telecommunication Systems*, Vol. 81, No. 4, 539–547, 2022.
 - [26] Arpaio, M. J., F. Fuschini, and D. Masotti, "A dual frequency blade antenna enabling UAV-based operations in ADS-B and 5G environments," in *2021 International Conference on Unmanned Aircraft Systems (ICUAS)*, 1618–1623, Athens, Greece, 2021.
 - [27] Akhter, Z., R. M. Bilal, and A. Shamim, "Dual-mode circular microstrip patch antenna for airborne applications," in *2021 15th European Conference on Antennas and Propagation (EuCAP)*, 1–5, Dusseldorf, Germany, 2021.
 - [28] Pham, D. A., M. Lee, and S. Lim, "High-gain conical-beam planar antenna for millimeter-wave drone applications," *IEEE Transactions on Antennas and Propagation*, Vol. 69, No. 10, 6959–6964, 2021.
 - [29] Seker, C. and M. T. Guneser, "Circular microstrip array antenna design for advance biomedical applications," in *2021 International Conference on Biomedical Innovations and Applications (BIA)*, 18–20, Varna, Bulgaria, 2022.
 - [30] Belen, A., E. Tetik, and H. Başak, "3D printed stacked antenna for WLAN drone communication," *Sigma: Journal of Engineering & Natural Sciences*, Vol. 41, No. 3, 2023.
 - [31] Reyna, A., J. C. Garza, L. I. Balderas, J. Méndez, M. A. Panduro, G. Maldonado, and L. Y. García, "Virtual antenna arrays with frequency diversity for radar systems in fifth-generation flying ad hoc networks," *Applied Sciences*, Vol. 14, No. 10, 4219, 2024.
 - [32] Salazar-Cerreno, J. L., S. S. Jehangir, N. Aboserwal, A. Segales, and Z. Qamar, "An UAV-based polarimetric antenna measurements for radar and communication systems from 3 GHz to 32 GHz," in *2021 IEEE Conference on Antenna Measurements & Applications (CAMA)*, 55–60, Antibes Juan-les-Pins, France, 2021.
 - [33] Carpenter, A., J. A. Lawrence, R. Ghail, and P. J. Mason, "The development of copper clad laminate horn antennas for drone interferometric synthetic aperture radar," *Drones*, Vol. 7, No. 3, 215, 2023.